# Performance of Optical Spatial Modulation and Spatial Multiplexing with Imaging Receiver

P.M. Butala, H. Elgala, T.D.C. Little
Department of Electrical and Computer Engineering
Boston University, Boston, Massachusetts
{*pbutala,helgala,tdcl*}*@bu.edu*

January 3, 2014

MCL Technical Report No. 01-03-2014

**Abstract**–Spatial modulation (SM) and spatial multiplexing (SMP) are two multiple-input multiple-output (MIMO) techniques for transmitting data over an indoor optical wireless channel. Receivers for SM and SMP can be of the non-imaging type, in which case the channel matrix coefficients can be highly correlated, or of the imaging type, which can reduce the degree of correlation and improve overall system performance. In this work, we propose a new framework to analyze the performance of imaging MIMO systems. This framework is applied to characterize the performance of SM and SMP under both imaging and non-imaging receivers. Results of our analysis indicate that imaging receivers can provide significant signal-to-noise ratio (SNR) improvements up to 45dB under SM and SMP as compared to the use of non-imaging receivers. Finally, the application of the proposed analysis framework indicates specific design principles to optimize imaging receiver parameters.

In *IEEE Wireless Communications and Networking Conference, Istanbul, Turkey, April 2014.*
*This work was supported primarily by the Engineering Research Centers Program of the National Science Foundation under NSF Cooperative Agreement No. EEC-0812056.*

# 1 Introduction

The rapid adoption of mobile computing devices with rich media capability is driving an apparently insatiable demand for wireless data capacity. Technological innovations in radio frequency (RF) communications have increased the capacity and utilization of available spectrum; however, various realities limit the capacity growth to match this demand. Optical wireless communications (OWC) with potential terahertz bandwidths have the potential to significantly increase available wireless capacity assuming that we overcome numerous implementation challenges.

We are particulary interested in visible light communications (VLC); a form of OWC that can exploit lighting devices (luminaires) as an opportunistic platform for indoor deployment. VLC in lighting is best achieved through the use of light-emitting diodes (LEDs) that are both energy-efficient, and are fast for the purpose of supporting intensity modulation (IM). This research area has foundations in OWC work outside of the visible spectrum, *i.e.* Infrared (IR) [1,2]. However, the alignment of demands for energy efficiency, the ubiquity of lighting as a deployment platform, and the spectrum crunch is creating new impetus for leveraging OWC for new capacity.

The technical challenges to enable OWC to realize its potential include (1) the limited modulation capabilities of lighting-grade LEDs, (2) the directional nature of light, which can be both a challenge and an opportunity, and (3) dealing with the complexity of an optical receiver, especially when it is mobile and must reconcile directional communications. The use of multiple channels to scale capacity using MIMO communications can address challenge (1). Challenge (2) is used as an opportunity to deliver desired properties at a receiver. Finally, at a macro level, challenge (3) is manageable through hybrid techniques described elsewhere; we isolate our operating environment to be in the context of indoor spaces – "smart rooms" – in which we can define limits of mobility and luminaire placement to achieve coverage and capacity goals.

MIMO techniques are considered to improve the capacity and throughput of the indoor OWC channel by distributing the signal power over multiple simultaneous links [3]. Repetition coding (RC), SMP and SM are three space-time techniques considered for MIMO OWC. In RC, each luminaire simultaneously transmits the same signal. For an M-ary modulation, RC offers spectral efficiency of $log_2(M)$ bits/s/Hz. In SM, the information is encoded spatially along luminaire index and along M-ary modulation over the indexed luminaire [4]. For $N_{tx}$ luminaires and M-ary modulation, SM offers spectral efficiency of $log_2(MN_{tx})$ bits/s/Hz. In SMP, information is jointly encoded using all luminaires. For $N_{tx}$ luminaires and M-ary modulation, SMP offers spectral efficiency of $log_2(M^{N_{tx}})$ bits/s/Hz.

A non-imaging receiver (NImR) can be modeled as a grid of photodiodes, each mounted with an optical concentrator and a filter. For an OWC channel deploying a NImR, the channel matrix coefficients are highly correlated causing the system performance to degrade significantly [5]. Performance of SM and SMP techniques using NImR has been studied recently and reported in reference [6]. In this prior work, the receiver elements are placed at a relatively wide distance – $10cm$ which would make this approach less practical for a small device such as a mobile phone. In contrast, we seek to achieve inter-element spacing on a chip scale using imaging receivers.

An imaging receiver (ImR) can be modeled as a grid of photodiodes sharing an imaging

lens and a filter. ImR has the potential to improve the system performance and increase the coverage areas while being incorporated in a handheld device. Imaging diversity receivers have been shown to markedly improve the performance of IR wireless communication systems [7] and indoor MIMO OWC systems [8]. In this paper, we propose an analysis framework including normalization steps that enables performance evaluation of SM and SMP approaches under ImR and NImR scenarios. We then study the effect of different system configurations and signal power tradeoff on the achievable BER performance using simulations.

The remainder of the paper is organized as follows. Section II presents a brief introduction on the SM and SMP systems. Section III introduces the normalization parameters for the generalized imaging system. Performance analysis results are presented in Section IV. Section V concludes the paper.

## 2 Imaging SM and SMP System

A simple optical MIMO system using an ImR for VLC applications is illustrated in Figure 1. Incoming data stream is coded and input to the modulator. The illumination state block provides a second input to the modulator which is the value of the average intensity to be emitted from each luminaire. Based on these inputs, the modulator block generates drive signals. $N_{tx}$ number of lumianires positioned on the ceiling act as optical transmitters while providing illumination. LEDs in the luminaire convert modulated data in the electrical domain into optical signals in the visible spectrum (E/O and conversely O/E conversion). These optical signals propagate through the indoor space and are incident on the receiver. The receiver performs O/E conversion. With apriori knowledge of the implemented modulation and coding schemes, the electrical signal is then demodulated and decoded to recover the transmitted information. Figure 2 illustrates a schematic of an ImR. The optical assembly consists of a filter, imaging lens, aperture and housing. $f$ is the focal length as set by the lens assembly. The sensor is made up of a matrix of $N_{px}$ contiguous pixels. The length of the shortest side of each pixel is $\alpha_{px}^{min}$ and the pixel diagonal is $\alpha_{px}^{max}$. The sensor is assumed to always be located distance $f$ away from the optical center of the lens.

The imaging optics acts as an optical demultiplexer. Based on the angle and the location of incidence, light rays are redirected by the imaging optics on to a specific path. This helps

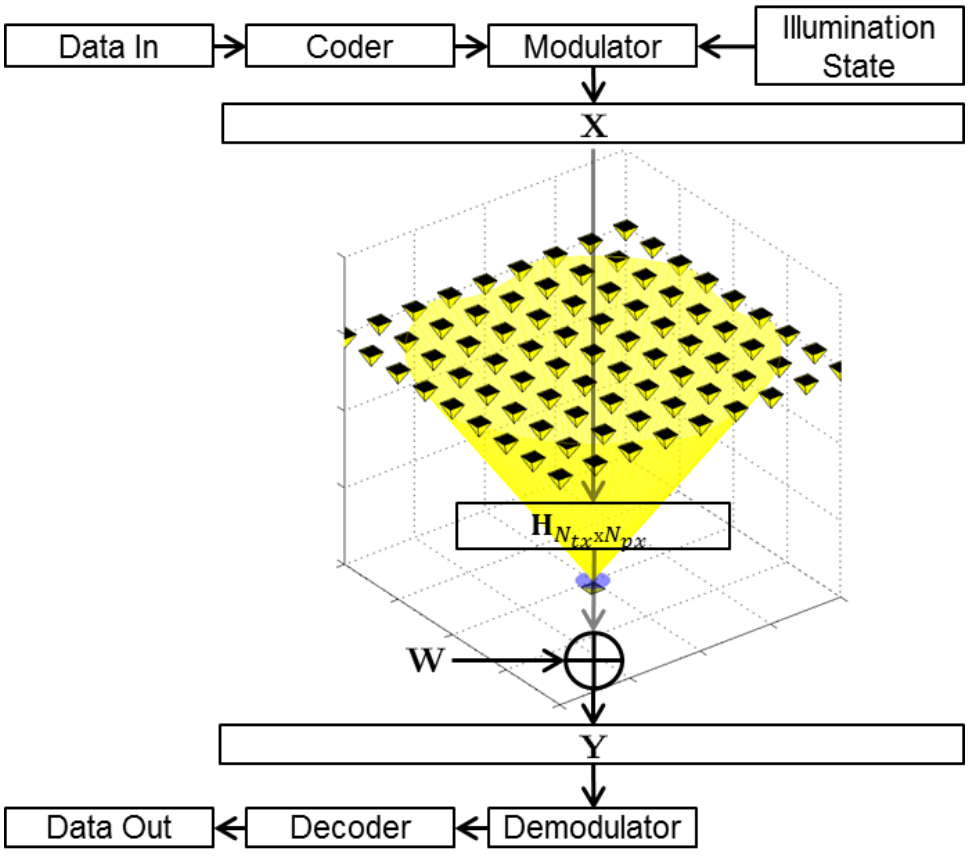


Figure 1: Schematic of an optical MIMO system.

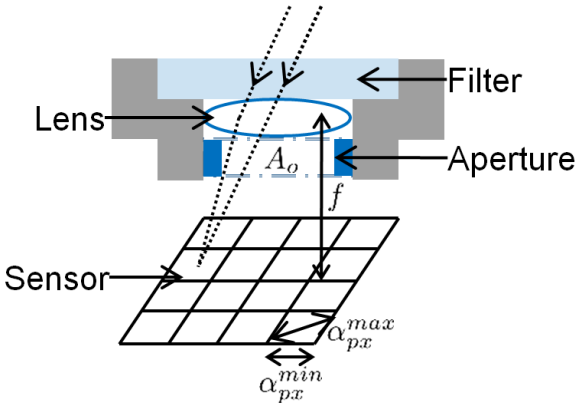


Figure 2: Schematic of an imaging receiver.

to decorrelate the channel matrix coefficients. Similarly, the ambient radiant flux incident at the aperture of the receiver is distributed among all pixels of the sensor. This helps to significantly reduce shot noise per pixel [9]. The channel can then be modeled as

$$\mathbf{Y} = \mathbf{HX} + \mathbf{W} \tag{1}$$

where $\mathbf{X}$ is the intensity modulated input signal vector of length $N_{tx}$. The channel matrix $\mathbf{H}$ takes into account the path-loss, transmission of the optics and the responsivity of the sensor pixels. It can be computed as in reference [8]. $\mathbf{Y}$ is the $N_{px}$ length output current vector. $\mathbf{W} \sim \mathcal{N}(\mathbf{0}, \sigma^2 \mathbf{I}_{N_{px}})$ is the additive white Gaussian noise (AWGN) vector.

SM encodes $k = log_2(N_{tx})$ bits in the transmitter index in addition to $m = log_2(M)$ bits using M-ary modulation. Thus SM achieves spectral efficiency of $r = k + m = log_2(MN_{tx})$ bits/s/Hz. The incoming data stream is divided into $r$ bits long symbols. First $m$ bits of each symbol are mapped to one of the M-ary constellation points while the last $k$ bits of each symbol select the luminaire that transmits the selected constellation point. SM implementation is illustrated in Figure 3a for $N_{tx} = 4$ transmitters and 4-PAM (pulse amplitude

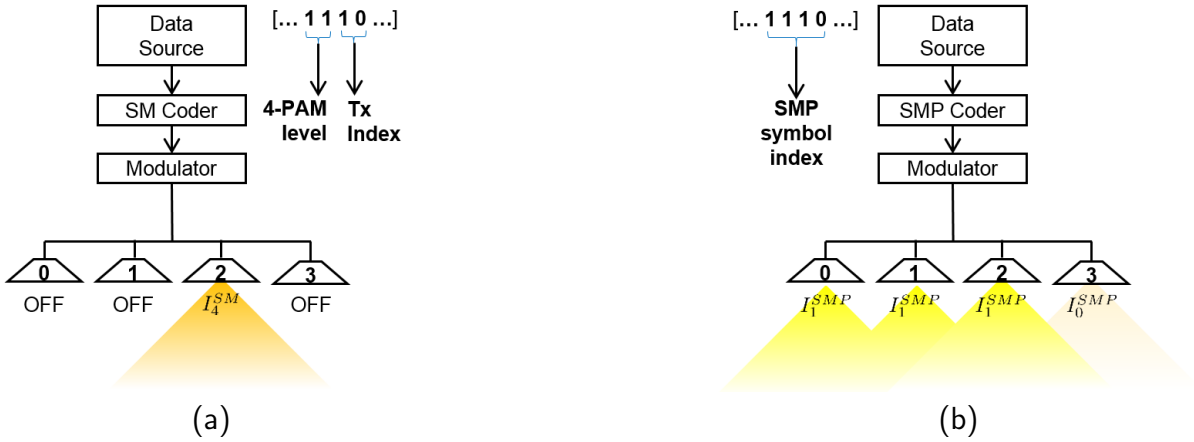


Figure 3: Illustration of (a) SM operation with $N_{tx} = 4$ and $M = 4$. (b) SMP operation with $N_{tx} = 4$ and $M = 2$.

modulation). M-PAM intensity levels for SM are selected as in (2) where $I_{avg}$ is the average signal constraint to maintain desired illumination. Given a bit sequence forming a symbol [1 1 1 0], PAM level 3 ($I_4^{SM}$) is sent on transmitter index 2.

$$I_x^{SM} = \frac{2I_{avg}}{M+1}x; x = 1 \dots M \tag{2}$$

On the other hand, SMP uses all luminaires to jointly transmit information. If each of the $N_{tx}$ luminaires can transmit M-ary modulation such that they jointly generate $M^{N_{tx}}$ unique symbols, spectral efficiency of SMP is given by $r = N_{tx}log_2(M)$ bits/s/Hz. Each $r$ bit long section of the incoming data stream is then mapped to one of the $M^{N_{tx}}$ unique symbols. SMP for a setup with $N_{tx} = 4$ transmitters and 2-PAM is illustrated in Figure 3b. M-PAM intensity levels for SMP are selected as in (3) where $I_{avg}$ is the average signal constraint to maintain desired illumination. A bit sequence forming a symbol [1 1 1 0] is jointly mapped to the $15^{th}$ out of $N_{tx}log_2(M) = 16$ possible unique symbols.

$$I_x^{SMP} = \frac{2I_{avg}}{M-1}x; x = 0 \dots M-1 \tag{3}$$

For a channel with equally likely symbols, a maximum likelihood detector is the optimal detector. If noise is AWGN, this reduces to nearest neighbor detection. Having observed $\mathbf{Y}$ and knowing $\mathbf{H}$, estimated symbol $\hat{\mathbf{X}}$ is the symbol closest to observation $\mathbf{Y}$ in Euclidean space. The signal detection can be written as

$$\begin{aligned} \hat{\mathbf{X}} &= \underset{\mathbf{X_i}}{\operatorname{argmax}}\, p_{\mathbf{Y}|\mathbf{X}}(\mathbf{Y}|\mathbf{X_i}, \mathbf{H}) \\ &= \underset{\mathbf{X_i}}{\operatorname{argmin}}\, ||\mathbf{Y} - \mathbf{H}\mathbf{X_i}||_F \end{aligned} \tag{4}$$

where $\mathbf{X_i}$ are the different symbols and $||.||_F$ is the Frobenius norm.

# 3 Analysis Framework

In this section, we develop a normalization framework to analyze performance of SM and SMP with ImR over a range of system configurations. The transmitters are assumed to be arranged on a regular grid, facing down, with pitch $P_{tx}$. Each transmitter has side length $\alpha_{tx}^{min}$ and diagonal $\alpha_{tx}^{max}$. The ImR surface is assumed parallel to the transmitter plane. A receiver at a distance $d$ from the transmitter plane sees a magnification $M_{im} = f/(d-f)$. The system performance is dependent on how the spots land on the pixel array. Different system configurations can generate similar spot profile on the sensor and thus giving similar performance. To analyze the system performance independent of a specific system configuration, the following normalization parameters are defined.

## 3.1 Normalized Luminaire Side Length

The normalized luminaire side length $\alpha_s$ is defined as the ratio of the diagonal of a spot to the side length of a pixel.

$$\alpha_s \equiv \frac{M_{im}\alpha_{tx}^{max}}{\alpha_{px}^{min}} \tag{5}$$

$\alpha_s$ specifies the spot size relative to the sensor dimensions. For example, consider two similar systems which differ in only the luminaire diagonal and the pixel side length. If both parameters differ in scale by the same factor, $\alpha_s$ would remain the same for both systems. $\alpha_s \leq 1$ implies that the spot size is at most as large as the size of a pixel. If the centroid of the spot is aligned with the centroid of a pixel, the spot will lie completely inside the pixel.

## 3.2 Normalized Luminaire Pitch

The normalized luminaire pitch $\delta_s$ is defined as the ratio of the spot pitch to the length of the pixel diagonal.

$$\delta_s \equiv \frac{M_{im}P_{tx}}{\alpha_{px}^{max}} \tag{6}$$

$\delta_s$ specifies the distance between the centroids of adjacent spots relative to the sensor dimensions. For example, consider two similar systems which differ in only the transmitter pitch and pixel diagonal. If both parameters differ in scale by the same factor, $\delta_s$ would remain the same. $\delta_s > 1$ ensures that centroids of adjacent spots lie on different pixels. In the limit, if both transmitters were point sources, condition $\delta_s > 1$ would ensure that different pixels receive signals from neighboring transmitters, thus eliminating inter-carrier interference (ICI).

## 3.3 Normalized Luminaire Edge-Edge Distance

The normalized luminaire edge-edge distance $\eta_s$ is defined as the ratio of minimum distance between the edges of adjacent spots to the length of the pixel diagonal.

$$\eta_s \equiv \frac{M_{im}(P_{tx} - \alpha_{tx}^{max})}{\alpha_{px}^{max}} \tag{7}$$

$\eta_s$ specifies the minimum possible distance between the edges of adjacent spots relative to the sensor dimensions. For example, now consider two similar systems which differ in only the minimum possible distance between the edges of adjacent luminaires and pixel diagonal. If both parameters scaled by the same factor, $\eta_s$ would remain the same. $\eta_s > 1$ ensures that adjacent spots do not overlap on any pixel. $\eta_s$ can be expressed in terms of $\alpha_s$ and $\delta_s$ as in (8b) where $l$ is conversion factor as in (8a). For square pixels, $l = 1/\sqrt{2}$.

$$l = \frac{\alpha_{px}^{min}}{\alpha_{px}^{max}} \tag{8a}$$

$$\eta_s = \delta_s - l\alpha_s \tag{8b}$$

## 3.4 Normalized Magnification

Let $M_0$ be the magnification of the system when $\alpha_s = 1$. Normalized magnification $\mu_s$ is defined as the ratio of the magnification of the system to $M_0$.

$$M_0 \equiv \frac{\alpha_{px}^{min}}{\alpha_{tx}^{max}} \tag{9a}$$

$$\mu_s \equiv \frac{M_{im}}{M_0} \tag{9b}$$

Consider two similar systems that differ in distance between the luminaire plane and the receiver and also in the receiver focal lengths. $\mu_s$ for both systems is the same value when both parameters differ in scale by the same factor.

In an indoor VLC system, luminaires need to maintain an average emitted radiant flux over different overlapping time windows so that the perceived illumination remains constant. Thus a fair performance comparison between different modulation schemes can be made when they emit the same radiant flux. Thus the SNR is defined as in reference [6],

$$SNR = \frac{(hP_{avg}^{tx})^2}{\sigma^2} \tag{10}$$

where $P_{avg}^{tx}$ is the average radiant flux emitted by a transmitter, $h$ is the O/E conversion factor ($AW^{-1}\Omega^{-2}$) and $\sigma^2$ is the noise power. Without loss of generality, $h = 1$ is assumed.

# 4 Results

The effects of varying transmitter array and ImR configurations on the BER performance of SM and SMP systems are studied using simulations. An array of 4 transmitters that are arranged on a regular grid with pitch $P_{tx}$ is considered. Using PAM, and to achieve 4 bits/sym, SM with $N_t = 4$ and $M = 4$ and SMP with $N_t = 4$ and $M = 2$ are implemented. To achieve 8 bits/sym, SM with $N_t = 4$ and $M = 64$ and SMP with $N_t = 4$ and $M = 4$ are implemented. The distance $d$ between the transmitter and receiver planes is $2m$. Lambertian luminaires of order $m = 1$ are assumed to have a spectral power distribution that is approximated by a sum of gaussians as in [10]. The responsivity of each pixel is equal to $0.4A/W$. Within this context, it is assumed that the pixels array is large enough to ensure that each of the four spots fall on the sensor for each of the different configurations considered below.

Using the parameters specified above, the channel gains are of the order of $10^{-7}$ for all simulations. Thus the transmitted signal power is about 140dB higher than the received signal power. Typically, the SNR is defined as the ratio of received signal power to noise power. However, given SNR as defined in (10), there is an offset of at least +140dB over typical definition.

## 4.1 Imaging vs Non-Imaging Receiver

Performance gains of using an ImR over a NImR are analyzed in this subsection. The transmitter and modulation parameters are the same as described above. For this analysis, $P_{tx} = 0.5m$ is considered. The NImR is made up of $2 \times 2$ array of pixels; each with a side length of $1mm$ and a pitch of $1mm$. Each pixel has a concentrator of refractive index 1.5 and field-of-view (FOV) of 60 deg. For the ImR, the sensor is modeled as $2 \times 2$ array of pixels with side length and pitch of $1mm$. The imaging lens is defined to have sufficient magnification to align the images of the four transmitters each with four pixels respectively. The FOV of the receiver changes with the sensor dimensions. The maximum FOV is defined as 60 deg; the same as in NImR case. A fair performance comparison between the two receiver configurations can be made under the assumption that the same signal radiant-flux is incident on both. Thus, the aperture of the ImR is modeled to have an area of $1mm^2$.

BER vs SNR curves for SM and SMP using NImR and ImR are shown in Figure 4. At low signal powers, using a NImR, shot noise is the dominant source of noise. At high signal powers, inter-channel-interference (ICI) dominates the noise for an NImR because the channel matrix coefficients are highly correlated. This can be seen as two regions of the BER curves when using a NImR. SM mitigates ICI and is thus more robust as compared to SMP in this scenario. BER achieved by SMP with NImR are greater than $10^{-3}$ for the range of SNR considered and thus cannot be improved by forward error correction (FEC). SM needs a high transmit signal power to achieve BER= $10^{-3}$ for both 4 and 8 bits/sym. Conversely, ImR completely demultiplexes the four transmit signals while generating a diagonal channel matrix and thus avoids ICI under ideal setup. To achieve BER= $10^{-3}$ at 4 bits/sym, SM with ImR performs about 8dB better that SMP with ImR and about 45dB better than SM with NImR. SMP packs more bits spatially in transmitter location as compared to SM. Thus, to achieve higher spectral efficiency while keeping the number of transmitters the

same, more PAM levels are needed for SM as compared to SMP thus quickly degrading SM's performance. To achieve BER= $10^{-3}$ at 8 bits/sym, SMP with ImR outperforms SM with ImR by about 10dB and SM with NImR by about 52dB. The channel matrix coefficient decorrelation afforded by ImR provide huge SNR gains over NImR for a given BER.

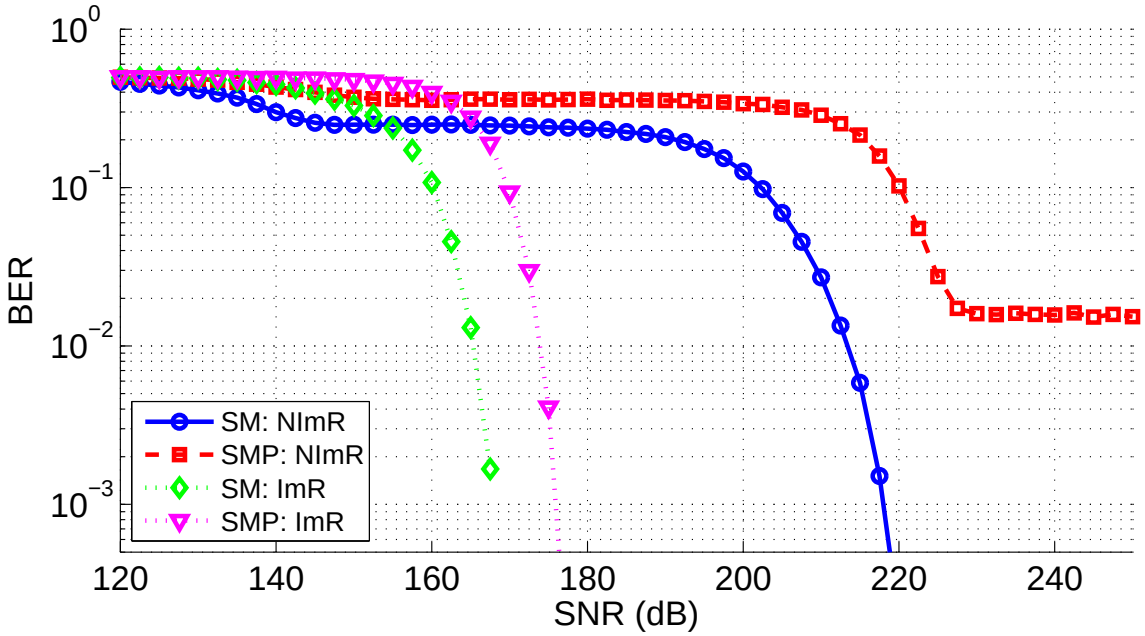


(a) 4 bits/sym

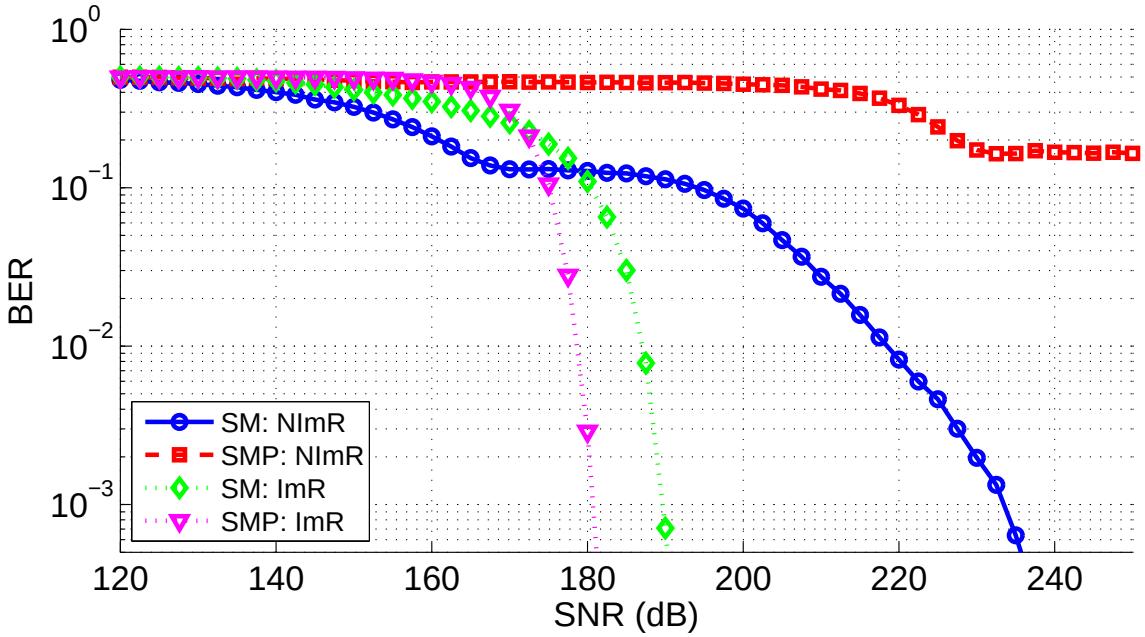


(b) 8 bits/sym

Figure 4: Performance comparison of SM and SMP using non–imaging and imaging receiver.

## 4.2 Varying $\alpha_s$

For this analysis, $\alpha_s$ is varied while keeping $\delta_s$ and $\mu_s$ fixed. As illustrated in Figure 5, $\alpha_s$ affects only the spot size. As $\alpha_s$ increases, spots on the sensor overlap increasingly more number of pixels degrading the BER performance. Increasing the number or pixels per spot also increases the noise for each link thus causing the drop in performance. Very small pixel sizes or very large transmitter sizes also cause increase in $\alpha_s$. A smaller pixel size does enable the system to pack more channels provided $\alpha_s$ is relatively small. On the other hand, having very small pixel sizes or alternately large transmitter illumination surface tend to increase $\alpha_s$ and force the system to operate in a suboptimal configuration.

BER vs SNR curves for SM and SMP for different values of $\alpha_s$ are shown in Figure 6. To achieve BER$\leq 10^{-3}$ at 4 bits/sym, SNRs of about [168,168,170,173]dB and [176,176,178,181]dB are needed for $\alpha_s$=[0.5,1,1.41,2] with SM and SMP respectively. To achieve BER$\leq 10^{-3}$ at 8 bits/sym, SNRs of about [190,190,192,195]dB and [181,181,183,186]dB are needed for $\alpha_s$=[0.5,1,1.41,2] with SM and SMP respectively. Thus there is about a 2dB SNR penalty for system operating at $\alpha_s = 1.41$ and 5dB SNR penalty for system operating at $\alpha_s = 2$ as compared to that at $\alpha_s = 1$.

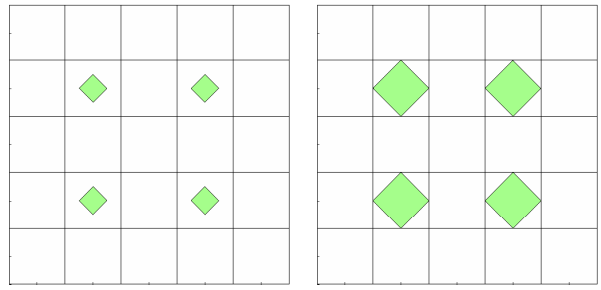

(a) $\alpha_s = 0.5$ (b) $\alpha_s = 1.0$

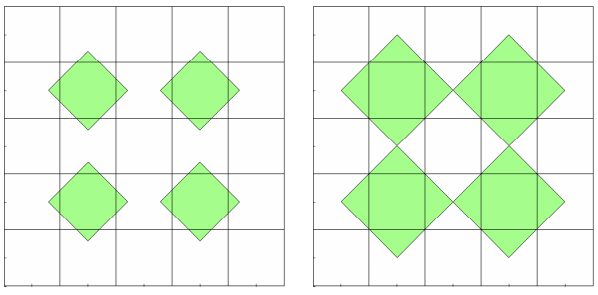

(c) $\alpha_s = 1.41$ (d) $\alpha_s = 2.0$

Figure 5: Spots on the sensor for different $\alpha_s$

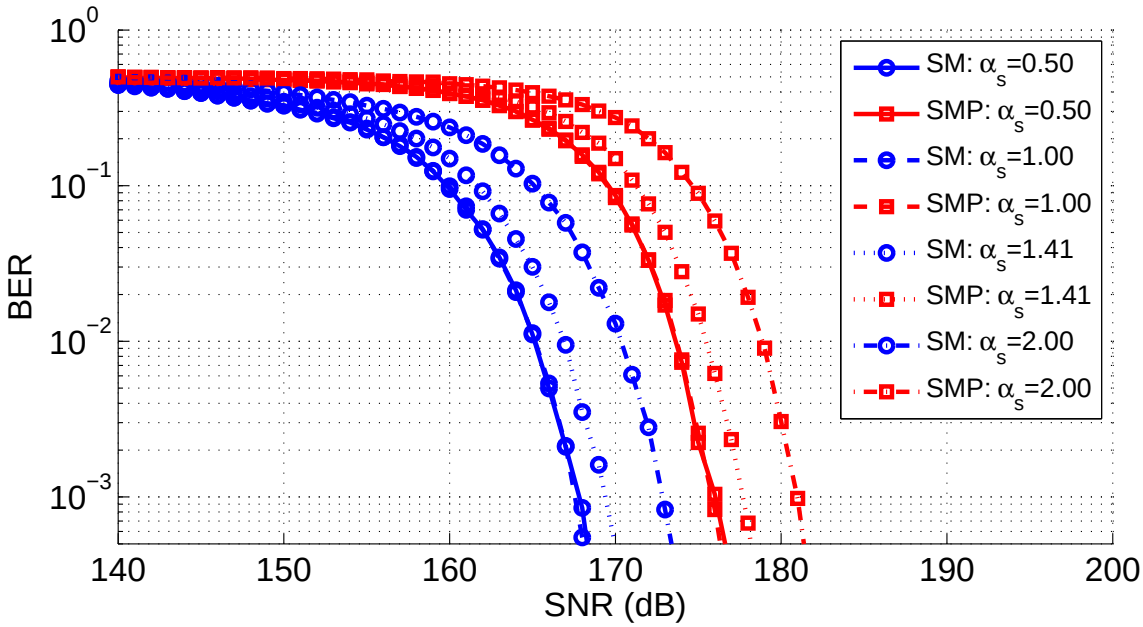


(a) 4 bits/sym

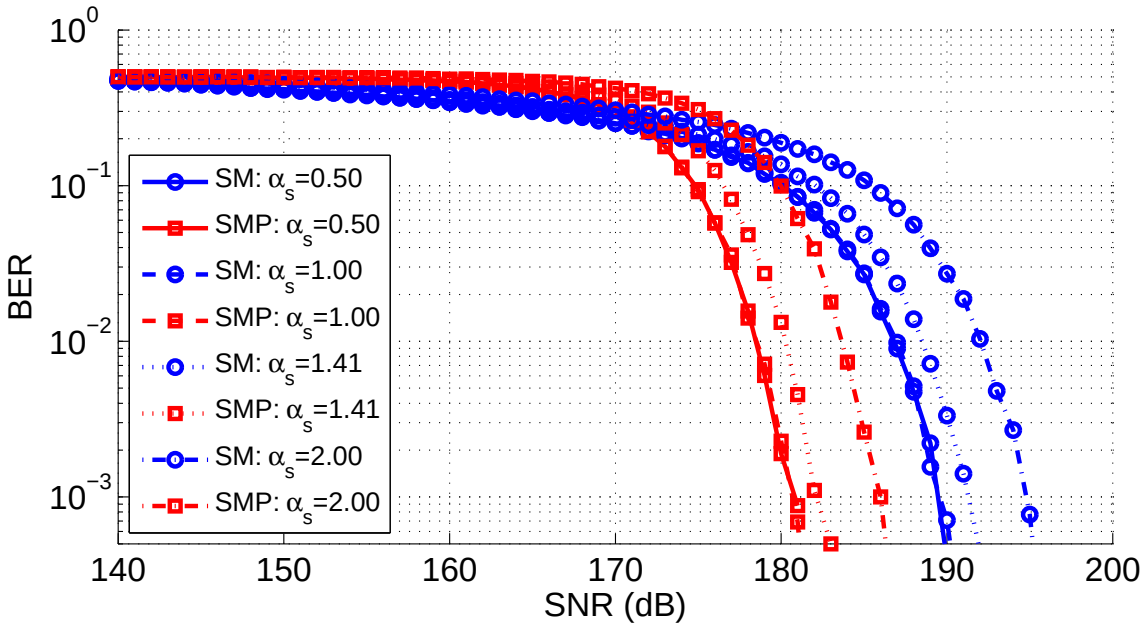


(b) 8 bits/sym

Figure 6: BER vs SNR for different $\alpha_s$.

### 4.3 Varying $\eta_s$

For this analysis, $\eta_s$ (alternately $\delta_s$) is varied while keeping $\alpha_s$ and $\mu_s$ fixed. Thus only the effect of change in spot pitch affects the BER performance. As illustrated in Figure 7, as $\eta_s$ increases, distance between the spots on the sensor increases as they push further apart.

BER vs SNR curves for SM and SMP for different values of $\eta_s$ are shown in Figure 8. To achieve BER$\leq 10^{-3}$ at 4 bits/sym, SNRs of about [167,174,172,170]dB and [175,182,180,178]dB are needed for $\eta_s$=[0,0.71,1,1.41] with SM and SMP respectively. To achieve BER$\leq 10^{-3}$ at 8 bits/sym, SNRs of about [189,196,194,192]dB and [180,187,185,183]dB are needed for $\eta_s$=[0,0.71,1,1.41] with SM and SMP respectively. We see that the BER performance is best when the spot overlaps minimum number of pixels and worst when the spot is centered at a corner of a pixel thus maximizing the number of pixels it overlaps with. In this setup, for BER= $10^{-3}$, there is an SNR penalty of about 7dB between the best and worst cases. The slight drop in performance for $\eta_s = 1.4$ as compared to $\eta_s = 0$ can be attributed to drop in free-space gain caused by the larger distance per link longer as a result of increased transmitter pitch.

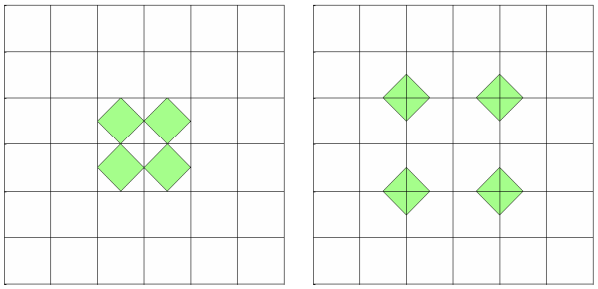

(a) $\eta_s = 0$ (b) $\eta_s = 0.71$

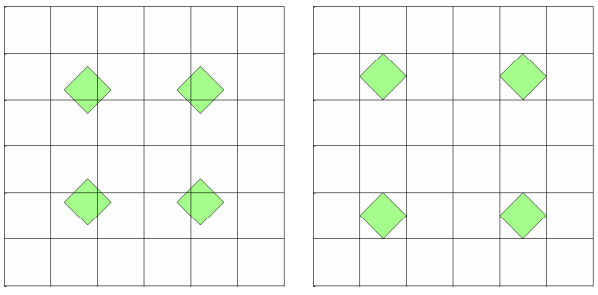

(c) $\eta_s = 1$ (d) $\eta_s = 1.41$

Figure 7: Spots on sensor for different $\eta_s$

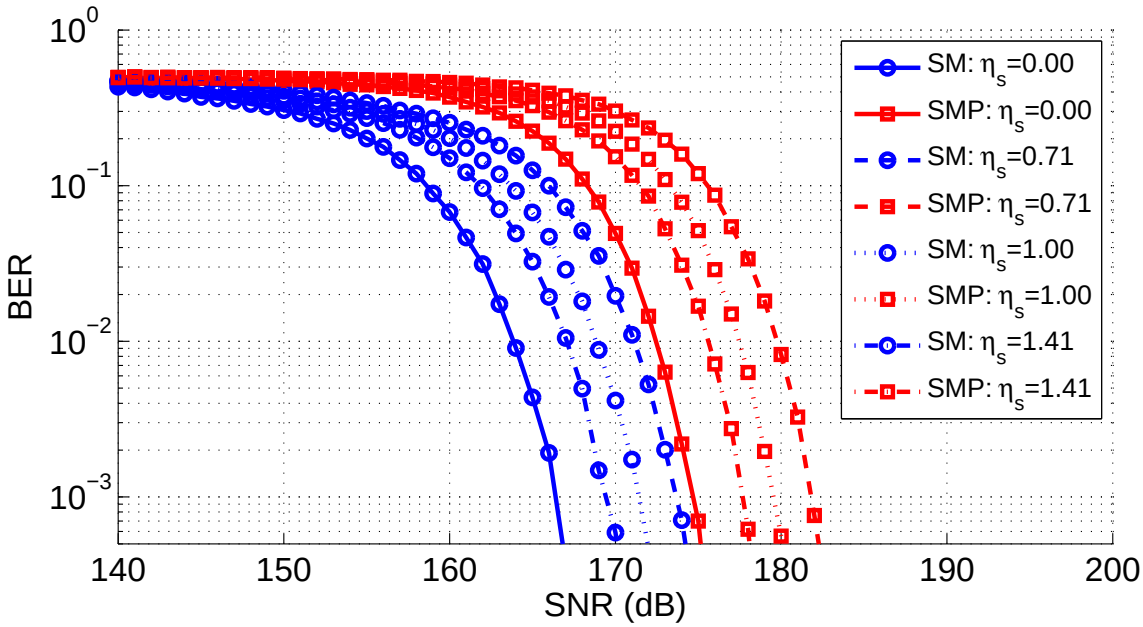


(a) 4 bits/sym

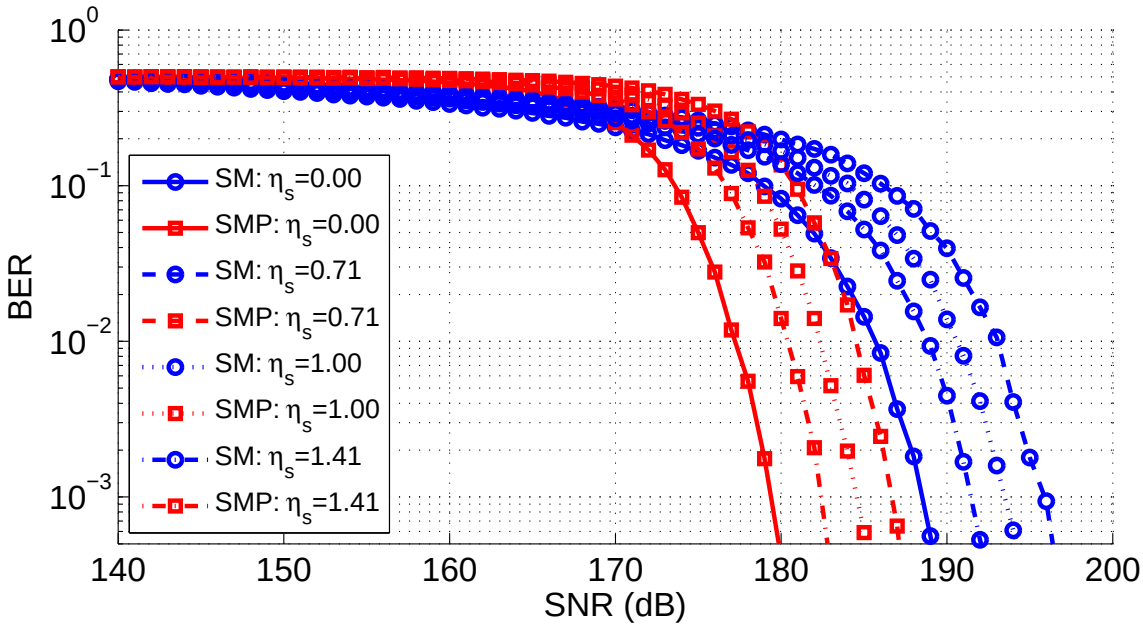


(b) 8 bits/sym

Figure 8: BER vs SNR for different $\eta_s$.

## 4.4 Varying $\mu_s$

In this analysis, $\mu_s$ is varied by varying $f$. Alternately, it can be varied by changing $d$. Varying $\mu_s$ affects both $\alpha_s$ and $\eta_s$ simultaneously. This captures their combined impact on the BER performance. We see from Figure 9 that increasing $\mu_s$ not only increases the spot size but also pushes the spots away from each other. Note unlike in previous case, the transmitter pitch remains constant ($P_{tx} > 0$).

BER vs SNR curves for SM and SMP for different values of $\mu_s$ are shown in Figure 10. To achieve BER= $10^{-3}$ at 4 bits/sym, SNRs of about [167,173,169,173]dB and [175,181,177,181]dB are needed for $\mu_s$=[0.5,1,1.41,2] with SM and SMP respectively. To achieve BER= $10^{-3}$ at 8 bits/sym, SNRs of about [189,195,191,195]dB and [180,186,182,186]dB are needed for $\mu_s$=[0.5,1,1.41,2] with SM and SMP respectively.

The best performance is obtained for $\mu_s \leq 0.5$. This is because at this value of $\mu_s$, $\alpha_s < 1$ and $\eta_s$ is such that all spots lie on different adjacent pixels. It can also be inferred that given enough transmitters in the room, at $\mu = 0.5$, every single pixel could get signal from a single transmitter thus greatly improving the capacity of the channel. If the luminaires transmit with different power levels or if the channels gains are significantly different, capacity maximizing $\mu_s$ is an optimization problem to be solved in the future.

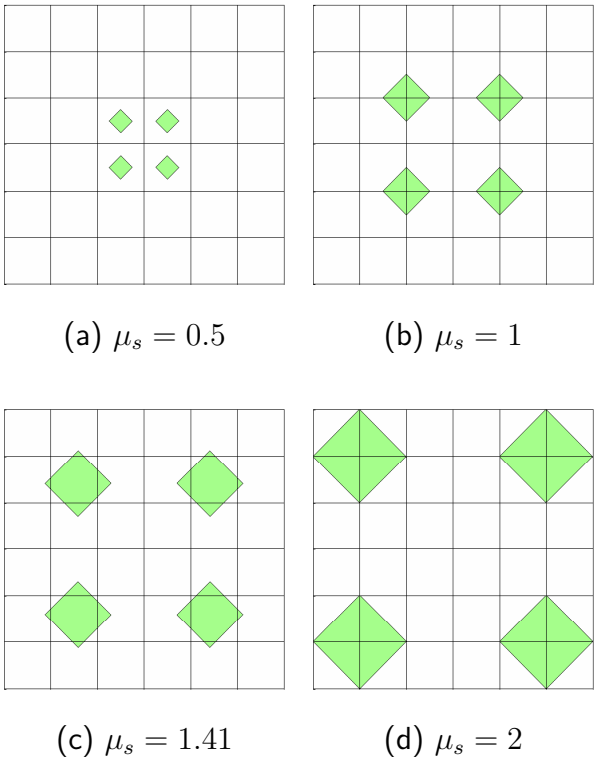

(a) $\mu_s = 0.5$ (b) $\mu_s = 1$

(c) $\mu_s = 1.41$ (d) $\mu_s = 2$

Figure 9: Spots on sensor for different $\mu_s$.

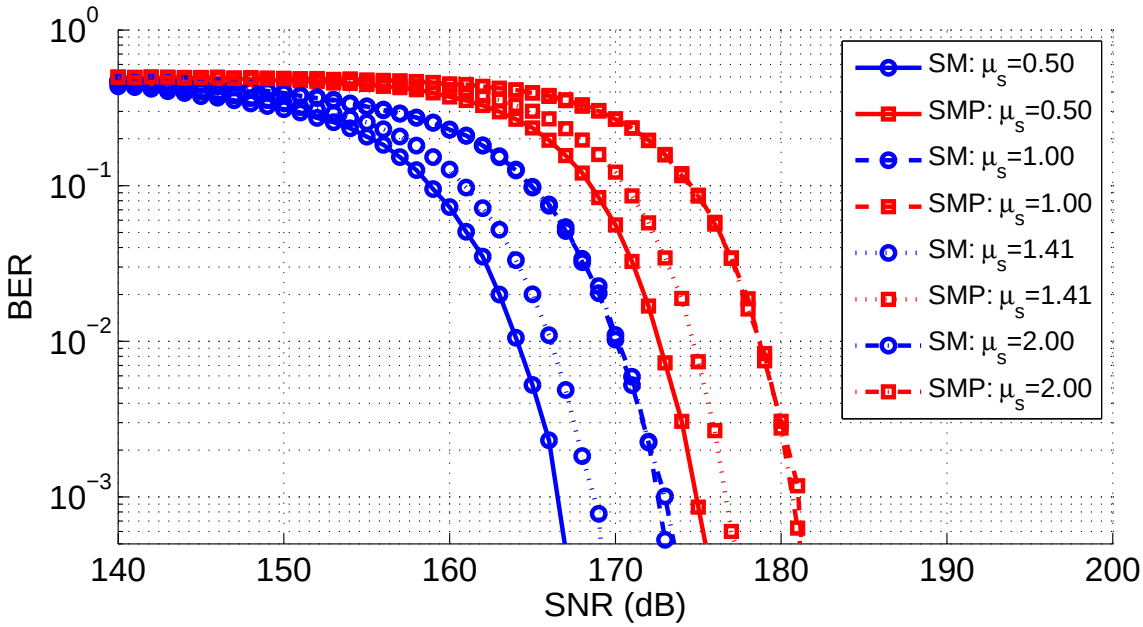


(a) 4 bits/sym

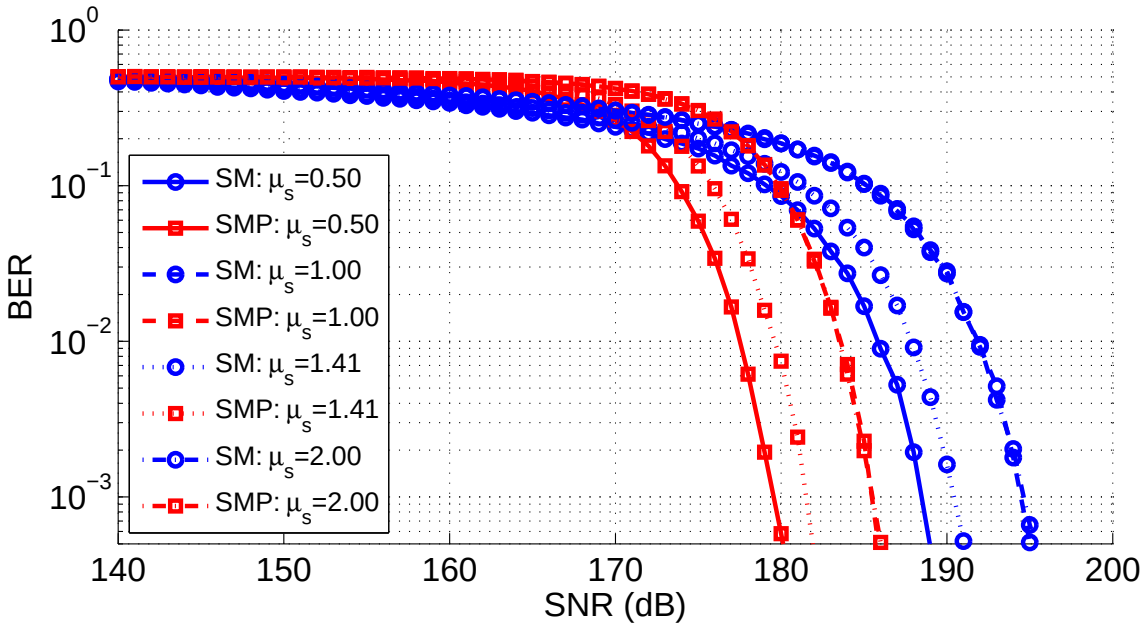


(b) 8 bits/sym

Figure 10: BER vs SNR for different $\mu_s$.

At lower bit rates, SM benefits from having higher transmit power per symbol at lower M-PAM level. To achieve higher bit-rates, higher M-PAM levels push the constellations closer to each other thus quickly degrading the SM performance as compared to SMP. As shown in Figure 6, Figure 8 and Figure 10, to achieve BER= $10^{-3}$, at 4 bits/sym, SM performs 8-10dB better while at 8 bits/sym, SMP performs 8-10dB better.

# 5 Conclusion

In this paper we explored the use of SM and SMP with both ImR and NImR in a MIMO VLC system. This effort was achieved via the creation of an analysis framework and normalization approach to enable performance characterization between systems. The results show that an ImR has the potential to provide significant SNR (≈45dB) gains over NImR for SM and SMP in a practical indoor scenario. For lower spectral efficiencies (4 bits/sym), SM performs 8-10 dB better than SMP while at higher spectral efficiencies (8 bits/sym), SMP gives 8-10 dB performance improvement. This is partly because the ImR helps decorrelate the parallel channel gains as compared to NImR. To achieve ideal performance for a given indoor configuration, parameters $\alpha_s$, $\eta_s$ and $\mu_s$ should be carefully selected. From the simulations we can conclude that the imaging MIMO system performs best when a spot is completely enveloped by a single pixel and adjacent spots each lie on adjacent pixels. For the simulation cases considered, $\alpha_s \leq 1$, $\eta_s = 0$ and $\mu_s = 0.5$ were found to provide the best system performance.

# References


[1] J. Kahn and J. Barry, "Wireless infrared communications," *Proceedings of the IEEE*, vol. 85, no. 2, pp. 265 –298, feb 1997.

[2] T. Komine and M. Nakagawa, "Fundamental analysis for visible-light communication system using led lights," *Consumer Electronics, IEEE Transactions on*, vol. 50, no. 1, pp. 100 – 107, feb 2004.

[3] H. Elgala, R. Mesleh, and H. Haas, "Indoor optical wireless communication: potential and state-of-the-art," *Communications Magazine, IEEE*, vol. 49, no. 9, pp. 56–62, 2011.

[4] R. Mesleh, H. Elgala, and H. Haas, "Optical spatial modulation," *Optical Communications and Networking, IEEE/OSA Journal of*, vol. 3, no. 3, pp. 234–244, 2011.

[5] L. Zeng, D. O'Brien, H. Minh, G. Faulkner, K. Lee, D. Jung, Y. Oh, and E. T. Won, "High data rate multiple input multiple output (mimo) optical wireless communications using white led lighting," *Selected Areas in Communications, IEEE Journal on*, vol. 27, no. 9, pp. 1654–1662, 2009.

[6] T. Fath and H. Haas, "Performance comparison of mimo techniques for optical wireless communications in indoor environments," *Communications, IEEE Transactions on*, vol. 61, no. 2, pp. 733–742, 2013.

[7] J. Kahn, R. You, P. Djahani, A. Weisbin, B. K. Teik, and A. Tang, "Imaging diversity receivers for high-speed infrared wireless communication," *Communications Magazine, IEEE*, vol. 36, no. 12, pp. 88 –94, dec 1998.

[8] P. M. Butala, H. Elgala, and T. D. Little, "SVD-VLC: a novel capacity maximizing VLC MIMO system architecture under illumination constraints," in *Globecom 2013 Workshop on Optical Wireless Communications*, Atlanta, USA, Dec. 2013.

[9] P. Djahani and J. Kahn, "Analysis of infrared wireless links employing multibeam transmitters and imaging diversity receivers," *Communications, IEEE Transactions on*, vol. 48, no. 12, pp. 2077–2088, 2000.

[10] J. Grubor, S. Randel, K.-D. Langer, and J. Walewski, "Broadband information broadcasting using led-based interior lighting," *Lightwave Technology, Journal of*, vol. 26, no. 24, pp. 3883–3892, 2008.